Article

Analysis of the Spatial and Temporal Distribution of Potential Evapotranspiration in Akmola Oblast, Kazakhstan, and the Driving Factors

Yusen Chen [1,2,3,†] **, Shihang Zhang** [1,2,4,†] **and Yongdong Wang** [1,2,3,*]

1   Xinjiang Institute of Ecology and Geography Chinese Academy of Sciences, Urumqi 830011, China
2   University of Chinese Academy of Sciences, Beijing 100049, China
3   National Engineering Technology Research Center for Desert-Oasis Ecological Construction, Urumqi 830011, China
4   State Key Laboratory of Desert and Oasis Ecology, Urumqi 830011, China
*   Correspondence: wangyd@ms.xjb.ac.cn; Tel.: +86-139-9915-0554
†   These authors contributed equally to this work.

Abstract: Potential evapotranspiration (PET) is the capacity of the sub-surface evapotranspiration process, which is determined by weather and climate conditions. As an important component of the surface energy balance and hydrological cycle, PET determines hydrothermal transport in surface ecosystems and is an important factor in regional water resource evaluation, water use efficiency, and drought prediction. Most of the existing studies have focused on the impact of PET on the ecological environment and regional climate, providing limited information on the characteristics of the regional distribution of potential evapotranspiration itself and the associated drivers. In this study, we use the Penman-Monteith (P–M) model to calculate the PET in Akmola Oblast, combined with relevant climate data, partial correlation analysis, and structural equation modelling (SEM) to investigate the spatial and temporal distribution characteristics of PET in the study area and its driving factors, as well as the influence of meteorological activity on PET after the implementation of the Green Ring Project in the capital area of Kazakhstan. The results of the study show that: (1) The PET in Akmola State presented a decreasing trend from 1991 to 2021, with a multi-year average value of 835.87 mm. There is large heterogeneity in the spatial distribution of PET, being significantly higher in the southwestern and northeastern regions of the study area than in the central region. (2) Simple and partial correlation analyses indicate that most of the correlations between meteorological and PET were significant, with strong spatial heterogeneity in the number of biased relationships between different meteorological activity and PET. The spatial characteristics of the correlations between PET and Srad (Solar radiation), VS (wind speed), and MAT (Mean annual temperature) were similar, with the strongest correlations observed in the southwestern part of Akmola State. Furthermore, the spatial distribution of the correlations between PET and SWC (soil water content) and ST (soil temperature) was similar, with stronger correlations in the central part of the study area than elsewhere. (3) The SEM demonstrated that the main drivers of PET change across the study area are Srad (0.59) and VS (0.37). In the metropolitan area, MAP (mean annual precipitation) is also a major driver of PET change, due to the implementation of the Green Ring Project, which has increased vegetation cover and improved the local environment. The results of this study highlight the impact of climate change on PET in Akmola Oblast, Kazakhstan, contributing to a better understanding of PET evolution and providing guidance for water management planning.

Keywords: potential evapotranspiration; partial correlation analysis; Penman-Monteith (P–M) model; climate change; structural equation modelling

1. Introduction

Drylands, which comprise hyper-arid, arid, semi-arid, and dry sub-humid climate zones, account for 47% of the world's geographical area and are home to 39% of the world's population [1]. Dryland ecosystems are more fragile and highly susceptible to climate change, with global semi-arid climate change escalating over the past 60 years. Global drylands are expanding due to global warming and intensive human activities, and changes in temperature and precipitation patterns have been observed in many parts of the world [2]). Increasing aridity is a major indicator of climate change in drylands globally [3], and total annual and seasonal potential evapotranspiration are increasing [4]. Drought results in soil moisture deficiencies [5] and declines in agricultural production, affecting the livelihoods of agriculturally reliant communities. Moreover, it contributes substantially to land degradation and biodiversity loss [6]), and multiple structural and functional characteristics of the ecosystem will be impacted [7]. Consequently, it is crucial to increase the monitoring and management of ecological settings in arid regions. Kazakhstan is the largest and most populous of the five Central Asian countries, and Akmola Oblast—where its capital, Nursultan, is located—in the steppes of Kazakhstan is the political and cultural center of Kazakhstan, as well as an important base for agriculture, forestry, and economic development. Its agricultural cultivation area accounts for one-fourth of Kazakhstan's national agricultural cultivation area, which has been undergoing dramatic expansion. Temperatures have risen at a rate of $0.4\,^\circ\mathrm{C}^{-10}\mathrm{yr}^{-1}$ in Central Asia over the past 30 years, which is significantly higher than in neighboring regions and the Northern Hemisphere as a whole ($0.3\,^\circ\mathrm{C}^{-10}\mathrm{yr}^{-1}$) [8]. This is likely to have extremely significant effects on the ecological quality of Akmola Oblast. During the same time period, different regions of Central Asia had severe droughts, and precipitation has exhibited large regionally diverse patterns and interannual variability [9]. In the context of global climate change, it is crucial to investigate changes in the geographical and temporal patterns of hydrological drought in the Akmola region. Evapotranspiration is a crucial process bridging the soil–vegetation–atmosphere continuum and serves as an essential link between Earth system components [10]. The mechanisms of evapotranspiration consist of evaporation from soil and moist plant surfaces, transpiration from plant leaves, and evaporation from plant surfaces [11]. In arid locations, as much as 90% of precipitation is returned to the environment by evapotranspiration [12]. Globally, evapotranspiration returns roughly 60% of precipitation to the atmosphere [13]. In the meantime, 50% of the solar radiation absorbed by the earth is converted into latent heat [14]. Potential Evapotranspiration (PET) is the capacity of the sub-surface evapotranspiration process, which is determined by weather and climate conditions. It is the theoretical upper limit of the actual evapotranspiration and has been widely used in agricultural water use studies, ecological process modeling, and evaluations of regional dry and wet conditions. Due to a substantial increase in temperature, PET production has increased in the dry regions of Asia (IPCC, 2013). A gradual decrease in precipitation has also been observed in the arid regions of West Asia [15]. The increase in PET and decrease in precipitation have led to decreased soil moisture, a decrease in the water table, and changes in land cover, ultimately leading to an expansion of the region's arid lands. PET not only affects ecosystems at the macro-scale, but also impacts natural animal life activities; for example, PET and temperature seasonality contribute 21.12% of the information required to predict the spatial distribution of stingless bees affecting Kenya [16]; furthermore, Taia et al. have investigated the effects of full irrigation (100% evapotranspiration, ETc) and deficit irrigation (80% ETc) of rice in the 2017 and 2018 seasons [17]. As a key component of the surface energy balance and hydrological cycle [18], PET governs the hydrothermal transport of surface ecosystems. Estimating continuous PET over extended time-series and assessing its geographical and temporal patterns and affecting factors are crucial for regional water resource appraisal, water usage efficiency, and drought prediction [10].

Most current PET measurement and estimation techniques are limited to a single-point scale, and do not represent a regional scale [12,19,20]. Based on the construction method, these models can be categorized as empirical or mechanical, and include the Penman-

Monteith, Stanghellini, Priestly–Taylor, Hargreaves, and Samani models [21]. Additionally, based on the contrast between soil evaporation and plant transpiration, these models can be split into single-source and dual-source models [22]. Due to its great accuracy, the Penman-Monteith (P–M) model has been utilized extensively. In recent years, climate warming has become more prominent, with a prominent effect on the ecohydrological cycle. Arid and semi-arid watersheds, as the watershed types experiencing the most significant ecohydrological changes, present large regional and seasonal differences in evapotranspiration trends. Prior research has focused primarily on the effects of PET on the regional variability of drought or on ecosystems, ignoring the characteristics and sources of PET's spatial and temporal variability. Nurdan, the capital of Kazakhstan, has been carrying out large-scale plantation forest construction projects for the past three decades. These projects have artificially altered the vegetation cover of Sultan and surrounding areas, which has had a significant effect on the local potential evapotranspiration [23]. In this paper, we use the Penman-Monteith (P–M) model to calculate the spatial and temporal variation of potential evapotranspiration (PET) in Akmola Oblast, Kazakhstan over the past three decades, as well as combining bias-off analysis and structural equation modeling (SEM) to calculate the driving effects of various environmental factors on PET changes.

The objectives of this paper are as follows:

1. Together with the P-M model, calculate and assess the spatial and temporal distribution characteristics of PET in Akmola State.
2. Using bias correlation analysis and SEM calculations, determine the sources of PET variance in the research area.

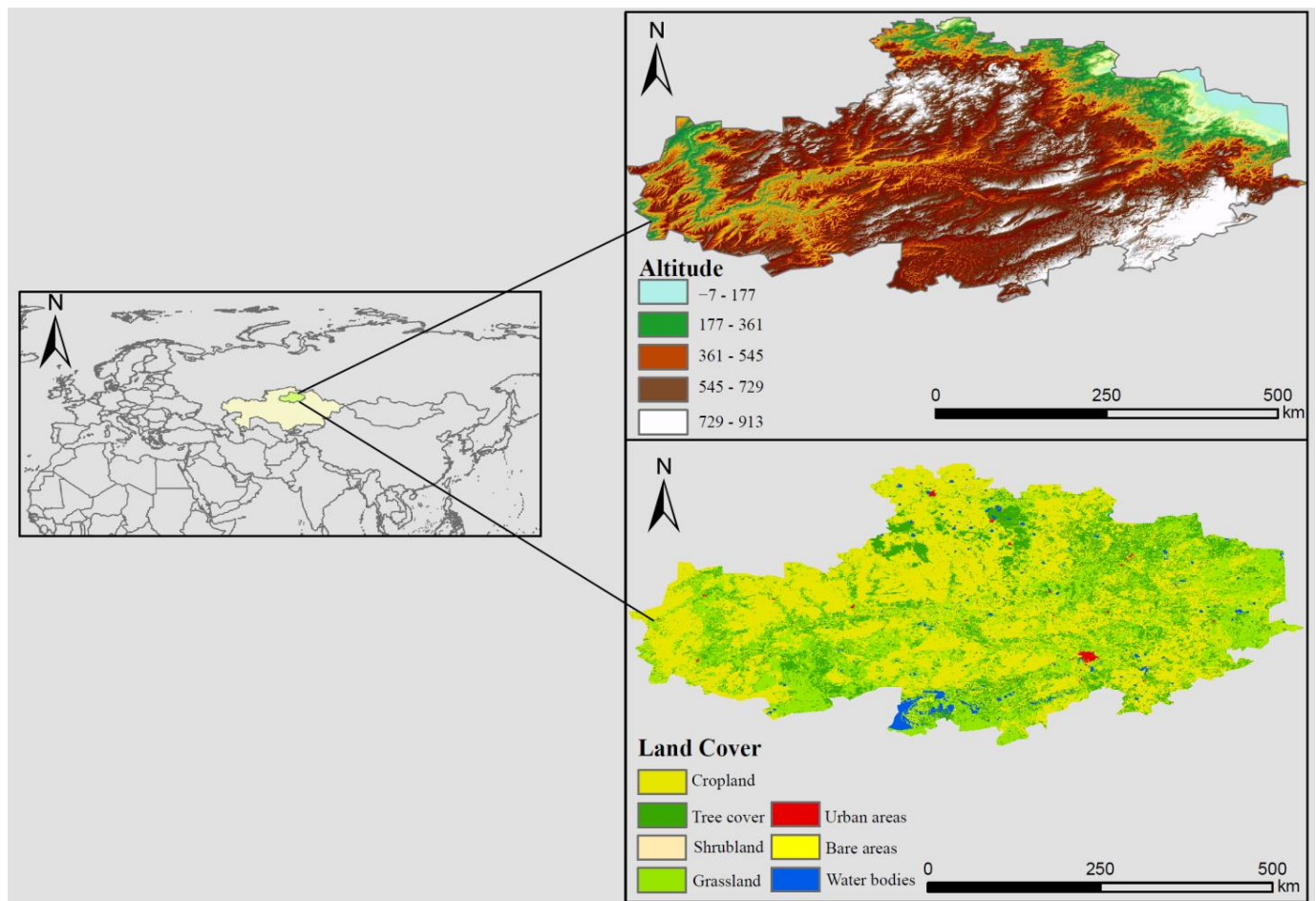Based on the preceding analysis, the following hypotheses are proposed:

1. As drought events occur frequently on a global scale and PET is a key indicator in drought monitoring and forecasting, we assume that PET in Alamok Oblast, Kazakhstan will continue to rise from 1991 to 2021 as a result of global warming.
2. PET is the theoretical upper limit of net surface evapotranspiration capacity, and we assume that solar radiation (Srad) is the most important meteorological driver of PET change.

2. Materials and Methods

2.1. Overview of the Study Area

We consider Akmola Oblast (49.9–53.8°N, 65.3–74.4°E) as the study area(Figure 1). Akmola Oblast is located in the upper reaches of the Khim River, in north-central Kazakhstan. It has an area of approximately 1.46×10^5 km^2, a population of approximately 747,600, an average altitude of 229 m, and an average annual precipitation of less than 500 mm. The average annual temperature in Akmola Oblast is between 2–6 °C. The lowest temperature in Winter may reach -41 °C. On its territory, the city of Nursultan is regarded as the second-coldest capital in the world.

From October until March of the following year, Akmola prefecture is covered in snow. Every year in April, the temperature rises and the snow melts. This provides favorable hydrothermal conditions, which are advantageous for the growth of crops. About 25% of Kazakhstan's agricultural land is devoted to grain cultivation in this region. It is a significant agricultural and forestry production center in the nation.

Figure 1. Overview map of the study area.

2.2. Data Sources

Google Earth Engine (GEE) is a highly developed cloud platform for the scientific processing of geographically relevant data. The Google Earth Engine platform contains an extensive repository of remote sensing data. We used the GEE platform to obtain the temperature and weather data necessary for the Penman-Monteith (P–M) model calculations. Furthermore, we downloaded land cover classification data of the study area from the ESA website (https://cds.climate.copernicus.eu/cdsapp#!/dataset/satellite-land-cover, URL (accessed on 25 August 2022)) with 300 m spatial resolution.

Terra Climate data is a global land surface monthly mean climate and climate water balance data set from 1958 to 2021, published by the University of Idaho (https://doi.org/10.1038/sdata.2017.191, URL (accessed on 25 August 2022)), with a spatial resolution of 4638.3 m. It encompasses global climate water balance and land surface climate data and consists of temperature-related information such as solar radiation (SRad), precipitation (MAP), surface temperature (MAT), wind speed (VS), and water vapor pressure (VPR).

We collected NDVI values by de-clouding and banding Landsat data, then supplemented and corrected the missing values with the NASA- and NOAA-published NOAA CDR AVHRR NDVI data set (https://doi.org/10.7289/V5PZ56R6, URL (accessed on 25 August 2022)), in order to study the contribution of vegetation cover to PET.

ALOS World 3D-30 m (AW3D30) is a global digital surface model (DEM) data set with a spatial resolution of approximately 30 m [24].

The aforementioned data were used for Penman-Monteith (P–M) computations in GEE by reprojection cropping procedures, among others, with respect to the years and spatial resolution of the data stated in Table 1.

Table 1. Area and proportion of different land cover types.

Land Cover Type	Areas (km^2)	Proportion (%)
Cropland	77,254.16	52.74
Tree cover	25,995.08	17.75
Shrubland	88.45	0.06
Grassland	39,868.47	27.22
Urban areas	526.48	0.36
Bare areas	235.13	0.16
Water bodies	2506.75	1.71

2.3. Computational Methods and Statistical Analysis

2.3.1. Penman-Monteith (P–M) Equation

The Penman–Monteith (P–M) equation, initially proposed by the Food and Agriculture Organization (FAO-56), is regarded as a standard method for estimating PET [25–28]. This method is a climatic data-based strategy that does not require calculation of other specific parameters and, as a result, may be applied globally (Zomer). In 1948, Penman was the first to combine radiant energy balance and aerodynamic mass transfer methods to derive equations for calculating evaporation from open water surfaces, based on standard climatic records of insolation, temperature, humidity, and wind speed. This integrated approach eliminated the need to measure the most difficult parameter: surface temperature [29]. The Penman-Monteith (P–M) equation for estimating PET is as follows:

$$ET_0 = \frac{\Delta(R_n - G) + \rho_a c_p \frac{(e_s - e_a)}{r_a}}{\Delta + \gamma\left(1 + \frac{r_s}{r_a}\right)},\tag{1}$$

where ET_0 is the evapotranspiration of the reference crop (in millimeters per day), R_n is the daily net crop surface radiation (in MJ m^{-2}), G is the soil heat flow density (in MJ m^{-2} day^{-1}), c_p is the specific heat of dry air at constant pressure, ρ_a is the air's density under constant air pressure, e_s is the saturated vapor pressure (in kPa), e_a is the actual vapor pressure (in kPa), $(e_s - e_a)$ is the saturated vapor pressure deficit (in kPa), Δ is the Vapor pressure slope curve (in kPa·°C^{-1}), γ is the wetness constant (in kPa·°C^{-1}), r_s is the surface resistance (in m/s), and r_a is the aerodynamic drag (in m/s).

2.3.2. Statistical Analysis

When two variables are simultaneously correlated with a third variable, bias correlation analysis is the process of removing the effect of the third variable and examining the degree of correlation between the other two variables. The R value of the correlation coefficient is the decisive factor: the greater the value of R, the more correlated the variables are; the lower the value, the lower the correlation.

$$R_{ij \cdot h} = \frac{r_{ij} - r_{ih} r_{jh}}{\sqrt{\left(1 - r_{ih}^2\right)\left(1 - r_{jh}^2\right)}},\tag{2}$$

where r_{ij} represents the simple correlation coefficient between x$_i$ and x$_j$, r_{ih} represents the simple correlation coefficient between x$_i$ and x$_h$, and r_{jh} represents the simple correlation coefficient between x$_j$ and x$_h$.

The null hypothesis for the test of the bias correlation coefficient is that the aggregate bias correlation coefficient between the two variables is 0. The following formula is applied in the *t*-test methodology:

$$t = \frac{\sqrt{n - k - 2} \cdot R}{\sqrt{1 - R^2}},\tag{3}$$

where R is the partial correlation coefficient, n is the number of sample observations, k is the number of controllable variables, and $n - k - 2$ is the number of degrees of freedom. The original hypothesis is rejected when $t > t_{0.05}(n - k - 2)$ or $p < 0.05$.
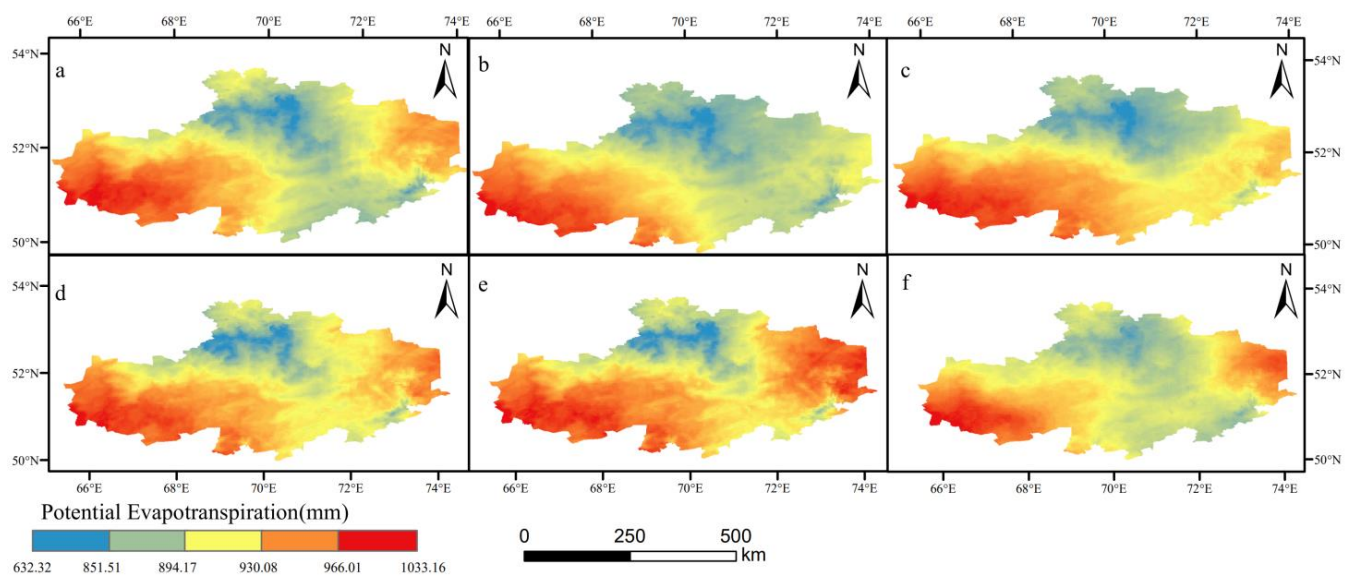
Compared with the traditional multivariate statistical method, structural equation modeling is based on the researcher's a priori knowledge of predetermined dependencies among factors in the system, which not only can discern the strength of the relationship between factors (path coefficients), but also can fit and judge the overall model, thus enabling a more comprehensive understanding of the natural system. In this study we used structural equation modeling (SEM) to analyze the direct and indirect effects of different environmental variables on PET by establishing an a priori SEMS to test the importance of multiple variables on PET, based on previous studies to determine the logical relationships between variables. Higher chi-square values (Chi square values) and higher p-values in the SEM indicated a better model fit [25]. The root mean square error of approximation (RMSEA) was equal to zero and the relative fit index (CFI) > 0.95 for the 90% confidence interval. We selected the best SEM as the one with the highest R^2 value for PET [26]. The "ggRandomForests" package in R (version 4.1.1, Peter Dalgaard, Professor, Statistical Center, Copenhagen Business School) was utilized to filter the covariance of environmental factors and rank the relative importance of random forests, in order to determine the relative contribution of each environmental element to the geographical variation of PET. The "lavaan" software was utilized to generate structural equation models (SEMs), in order to study the principal causes of spatial variation of PET in Akmola State.
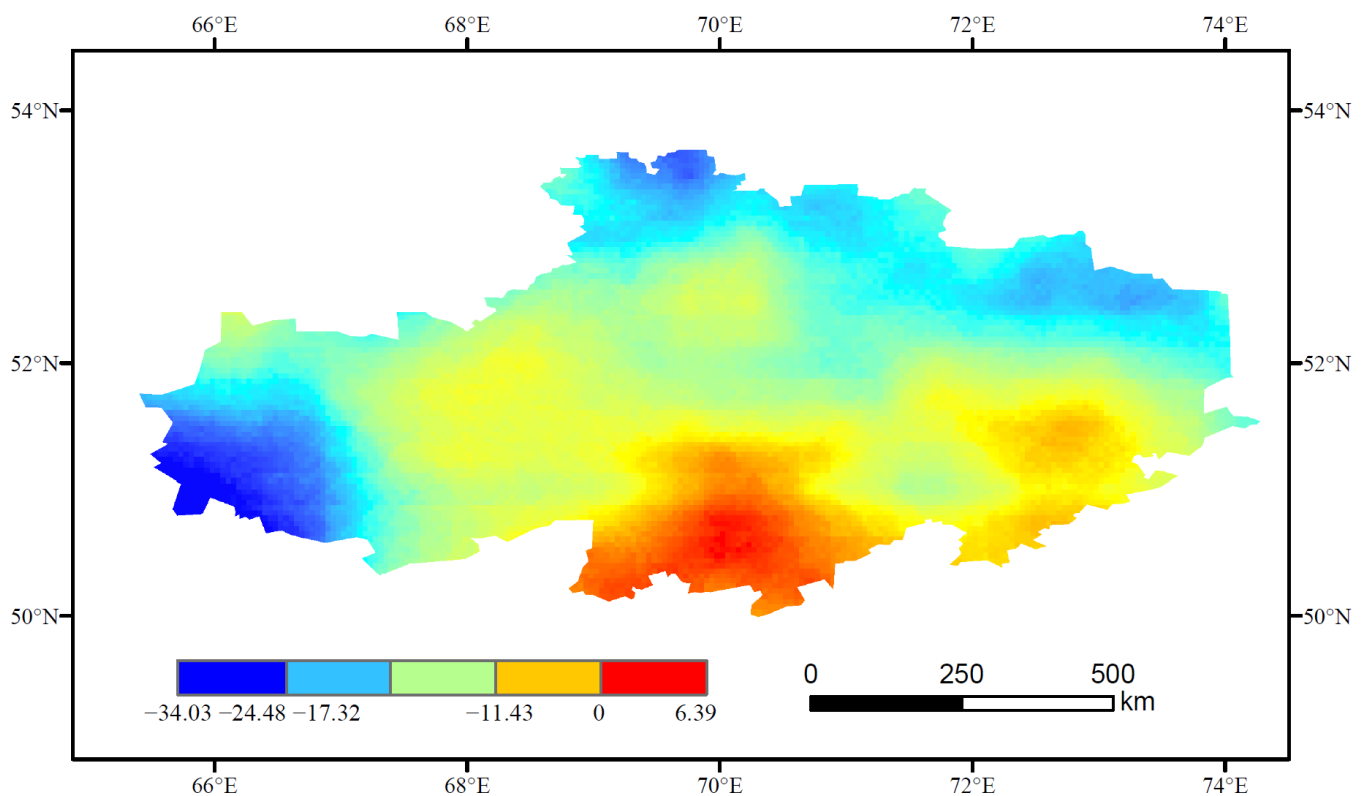
3. Results and Analysis

3.1. Spatial and Temporal Distribution Characteristics of PET in Akmola State

Figure 2 depicts the regional distribution of potential evapotranspiration in the study area from 1991 to 2021 in Akmola Oblast, Kazakhstan. This report includes data on potential evapotranspiration outcomes for five time periods: 1991, 1998, 2005, 2013, and 2021. The spatial distribution characteristics of potential evapotranspiration in the region generally varied consistently throughout the study period. Figure 2a–e demonstrate that the annual mean PET presented substantial regional variability and was generally similar to the distribution of wind speed, solar radiation, and soil temperature gradients, with a pattern of high values in the east and west and low values in the center and north. From 1991 to 2021, the multi-year average value of Akmola Oblast's potential evapotranspiration was 837.99 mm ($\pm$160), the precipitation was higher in the northern part of Akmola Oblast in the Huichinsk region and the central part of Akko compared to other regions, and the wind speed, solar radiation, and soil temperature were lower than in other regions. In the eastern and western portions of the study area, the predominant land cover types are arable land, grassland, and bare land; the climate is windy year-round; solar radiation is high; and the average annual potential evapotranspiration is greater than 900 mm, with the highest value exceeding 1000 mm.

As shown in Figure 3, Tables 2 and 3, in Akmola Oblast, only 6.39% of the regions presented an increase in potential evapotranspiration from 1991–2021, located in Imeni Kostycheva in the western part of the oblast and Kokshetau and Valikhanovo in the northern part of the oblast, with the highest interannual variation rate of 6.39 mm/yr. The regions with a decrease in annual potential evapotranspiration in the study area accounted for a relatively small annual rate of change in PET in the study area. Overall, the PET in the study area showed a decreasing trend (Figure 3i), and the PET fluctuated more frequently in magnitude and trend over time.

Figure 2. Spatial and temporal distribution of PET in Akmola State (**a**–**f**), representing the spatial and temporal distribution of PET in Akmola State in 1991, 1997, 2003, 2009, 2016, and 2021.

Figure 3. Average annual rate of change in PET in Akmola State, 1991–2021.

Table 2. Data sources and basic parameters.

Type	Variable	Abbreviations	Unite	Original Resolution	Data Source
Climate	Mean annual temperature	MAT	°C	4638.3 m	https://doi:10.1038/sdata.2017.191 (accessed on 20 September 2022)
	Mean annual precipitation	MAP	mm	4638.3 m	https://doi:10.1038/sdata.2017.191 (accessed on 20 September 2022)
	Aridity	-	-	4638.3 m	https://doi:10.1038/sdata.2017.191 (accessed on 20 September 2022)
	Maximum temperature	-	°C	4638.3 m	https://doi:10.1038/sdata.2017.191 (accessed on 20 September 2022)
	Minimum temperature	-	°C	4638.3 m	https://doi:10.1038/sdata.2017.191 (accessed on 20 September 2022)
	vapor pressure difference	VPD	kPa	4638.3 m	https://doi:10.1038/sdata.2017.191 (accessed on 20 September 2022)
	Solar radiation	Srad	W/m^2	4638.3 m	https://doi:10.1038/sdata.2017.191 (accessed on 20 September 2022)
	Wind speed	vs	m/s	4638.3 m	https://doi:10.1038/sdata.2017.191 (accessed on 20 September 2022)
	Soil water content	SWC	mm	4638.3 m	https://doi:10.1038/sdata.2017.191 (accessed on 20 September 2022)
	Soil temperature	ST	°C	11,132 m	https://doi:10.5067/5NHC22T9375G (accessed on 20 September 2022)
NDVI	NDVI	-	-	30 m	https://glovis.usgs.gov/ (accessed on 20 September 2022)
Elevation	Elevation	-	m	30 m	https://www.eorc.jaxa.jp/ALOS/en/aw3d30/data/index.htm (accessed on 20 September 2022)

Note: All abbreviations in this manuscript are consistent.

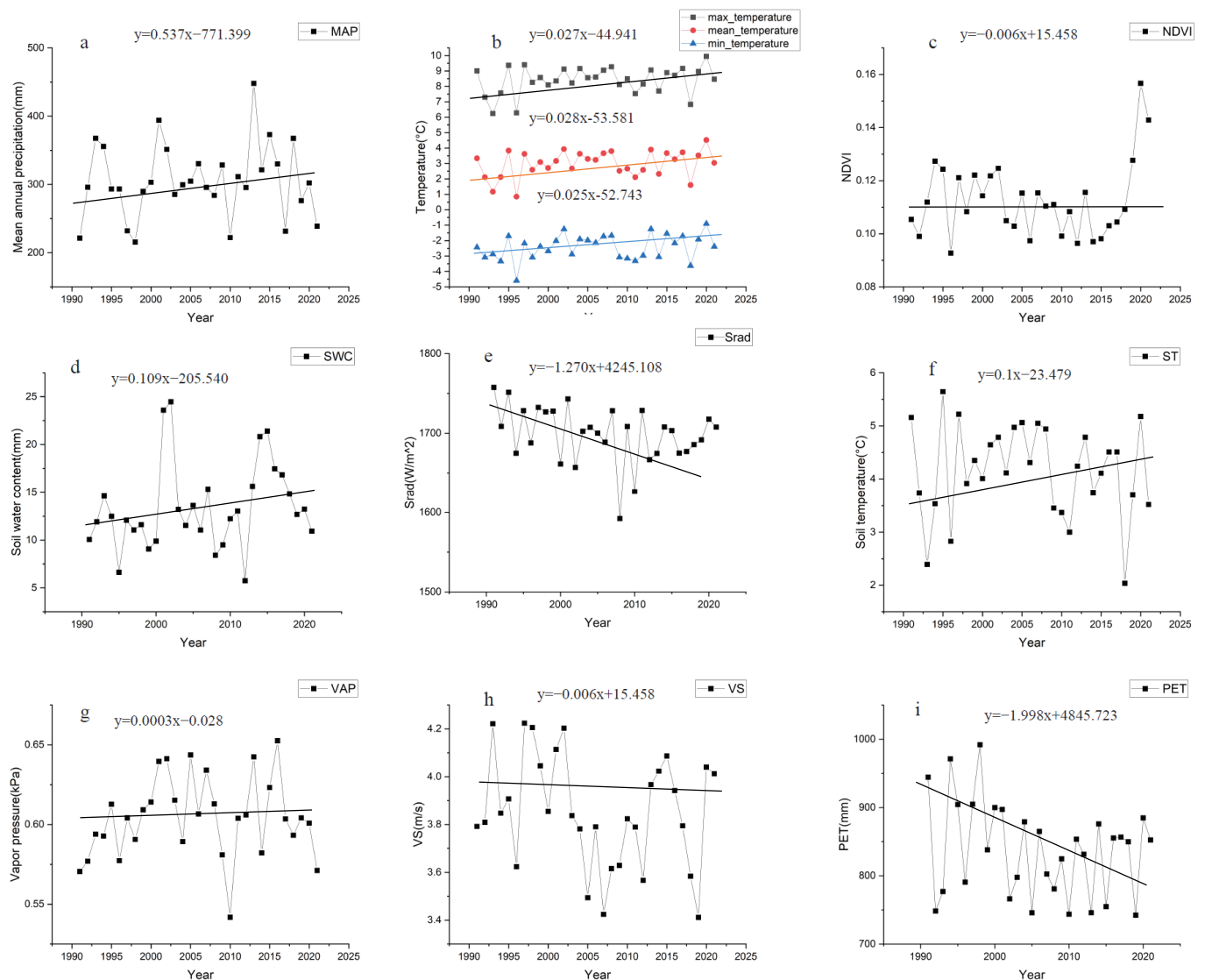**Table 3.** Percentage of annual average change in PET in Akmola State.

Interannual Rate of Change (mm/yr)	Area (km^2)	Percentage (%)
−34.03−−24.48	14,144.43	9.62%
−24.28−−17.32	38,654.57	26.29%
−17.32−−11.43	44,050.63	29.96%
−11.43–0	40,786.53	27.74%
0–6.39	9395.311	6.39%

3.2. Drivers of Spatial and Temporal Variability of Potential Evapotranspiration

3.2.1. Spatial and Temporal Distribution Characteristics of Environmental Factors in Akmola State

The meteorological parameters and soil data for the state of Akmola from 1991 to 2021 are depicted in Figure 4. The average annual precipitation in the research area was 305.153 mm (±90), with increasing interannual variance (Figure 4a) and a significant west–east tendency in geographical distribution (Figure 5). The average annual precipitation north of the study area was less than 300 mm, whereas the highest multi-year average was more than 360 mm in the south. The region's multi-year mean annual temperature was 2.98 °C (±1.54), with a steady increase in spatial distribution from north to south (Figure 4b), showing a minimum of 1.69 °C in the northern portion of Akmola State and a maximum of 4.48 °C in the southwestern portion of the study area (Figure 5b). The NDVI values in the study area did not change significantly from 1991 to 2021, with a multi-year average value of 0.11 (±0.003), without a significant trend of increase or decrease (Figure 4c). Spatially the NDVI showed a different distribution of vegetation cover, with higher vegetation cover and higher NDVI values in the northern part of Akmola Oblast, around the Huichinsk area and the Ishim River basin, whereas the rest of the areas were dominated by low values (Figure 5c).
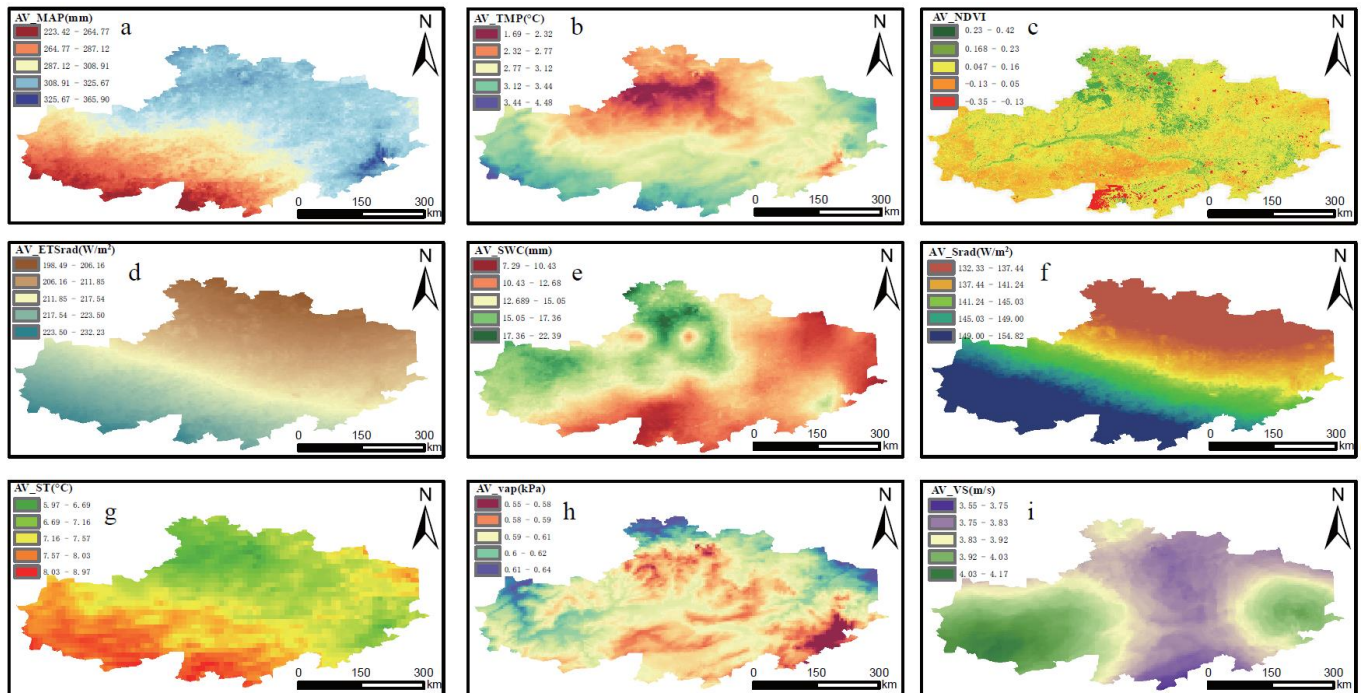
Figure 4. Environmental variables: (**a**) average annual precipitation; (**b**) average annual temperature, annual maximum temperature and annual minimum temperature; (**c**) NDVI; (**d**) soil water content; (**e**) solar radiation; (**f**) soil temperature; (**g**) differential vapor pressure; (**h**) wind speed; and (**i**) potential evapotranspiration during 1991–2021.

The multi-year mean soil water content in the study area was 12.89 m^3/m^3, which did not vary significantly in the time-series (Figure 4d). However, there was significant spatial heterogeneity (Figure 5e), the soil water content northwest of the study area was generally greater than 15.05 m^3/m^3, significantly greater than that in the southeast of study area (with soil content generally less than 10.43 m^3/m^3). The multi-year mean value of solar radiation in the research area was 1710.33 W/m^2 (±110), with increasing variation over time (Figure 4f), and the geographical distribution exhibited features of high in the southwest and low in the northeast (Figure 5f). The multi-year mean value of soil temperature was 4.15 °C (±1.5), with an increasing trend (Figure 4f) and, in spatial distribution, with the Isim River as the boundary, the multi-year mean value of soil temperature was greater than 7.57 °C to the southwest of the Akmola State and less than 6.69 °C to the northeast of the Akmola State (Figure 5g). The multi-year mean pressure difference in the research area was 0.60 kPa (±0.05), with no interannual variation (Figure 4g) and no obvious pattern of spatial distribution (Figure 5h). The multi-year mean wind speed in Akmola oblast was 3.85 m/s (±0.4), with considerable interannual variation (Figure 4h), and geographical

characteristics of higher in the east and west (more than 3.92 m/s) and lower in the middle (less than 3.83 m/s; Figure 5i).

Figure 5. Spatial distribution of environmental factors in Akmola State: (**a**) average annual precipitation; (**b**) average annual temperature; (**c**) NDVI; (**d**) potential solar radiation; (**e**) soil water content; (**f**) solar radiation values; (**g**) soil temperature; (**h**) vapor pressure values; and (**i**) wind speed.

3.2.2. Analysis of the Correlation between Potential Evapotranspiration and Various Climatic Parameters in Akmola State
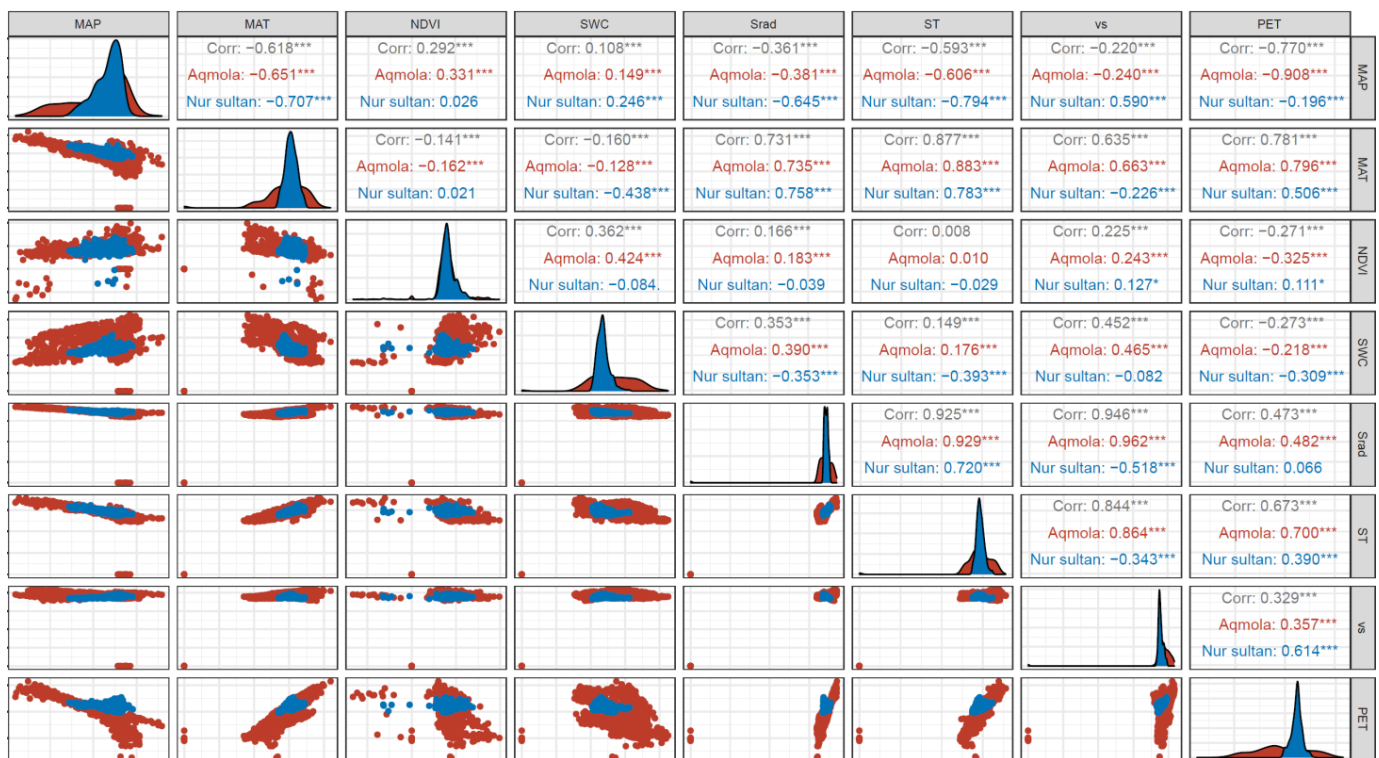
There are numerous climatic elements that influence PET. In particular, climate change influences PET in a variety of ways, including through increased air flow above the surface, increased in temperature, alterations to air humidity, and land-use change (e.g., the expansion of forest cover influences the local microclimate cycle). To quantify the effects of numerous factors on PET, a comparative analysis of PET and several influencing factors in the study region was carried out.

As shown in Figure 6, the simple correlations between PET and MAP, NDVI, and SWC within the state of Akmola were significantly negative ($p < 0.001$), with correlation coefficients of −0.908, −0.325, and −0.218, respectively, whereas the simple correlations between PET and MAT, Srad, ST, and VS were significantly positive ($p < 0.001$), with correlation coefficients of 0.796, 0.482, 0.700, and 0.357, respectively. However, the correlations between PET and numerous climate parameters in the metropolitan region were slightly varied, as were the correlation coefficients and the simple connection between NDVI and PET, which was positive with a correlation coefficient of 0.111.

3.2.3. Spatial Distribution of Potential Evapotranspiration and Environmental Factor Bias off in Akmola State

In view of the different correlations exhibited between PET and impact factors in Akmola State and the metropolitan area within its territory, we found that different regions had different correlations between PET and the various impact factors. Therefore, in order to explore the spatial distribution characteristics of climate factors that play a major role in PET changes, we calculated the partial correlation coefficients between potential evapotranspiration and the different impact factors at the level of α = 0.05. The significance test was performed at the level of α = 0.05 to exclude the mutual influence between different

elements and to select the elements closely related to PET; the results for factors passing the significance test are shown in Figure 7.

	MAP	MAT	NDVI	SWC	Srad	ST	vs	PET	
	(distribution)	Corr: −0.618*** Aqmola: −0.651*** Nur sultan: −0.707***	Corr: 0.292*** Aqmola: 0.331*** Nur sultan: 0.026	Corr: 0.108*** Aqmola: 0.149*** Nur sultan: 0.246***	Corr: −0.361*** Aqmola: −0.381*** Nur sultan: −0.645***	Corr: −0.593*** Aqmola: −0.606*** Nur sultan: −0.794***	Corr: −0.220*** Aqmola: −0.240*** Nur sultan: 0.590***	Corr: −0.770*** Aqmola: −0.908*** Nur sultan: −0.196***	MAP
		(distribution)	Corr: −0.141*** Aqmola: −0.162*** Nur sultan: 0.021	Corr: −0.160*** Aqmola: −0.128*** Nur sultan: −0.438***	Corr: 0.731*** Aqmola: 0.735*** Nur sultan: 0.758***	Corr: 0.877*** Aqmola: 0.883*** Nur sultan: 0.783***	Corr: 0.635*** Aqmola: 0.663*** Nur sultan: −0.226***	Corr: 0.781*** Aqmola: 0.796*** Nur sultan: 0.506***	MAT
			(distribution)	Corr: 0.362*** Aqmola: 0.424*** Nur sultan: −0.084.	Corr: 0.166*** Aqmola: 0.183*** Nur sultan: −0.039	Corr: 0.008 Aqmola: 0.010 Nur sultan: −0.029	Corr: 0.225*** Aqmola: 0.243*** Nur sultan: 0.127*	Corr: −0.271*** Aqmola: −0.325*** Nur sultan: 0.111*	NDVI
				(distribution)	Corr: 0.353*** Aqmola: 0.390*** Nur sultan: −0.353***	Corr: 0.149*** Aqmola: 0.176*** Nur sultan: −0.393***	Corr: 0.452*** Aqmola: 0.465*** Nur sultan: −0.082	Corr: −0.273*** Aqmola: −0.218*** Nur sultan: −0.309***	SWC
					(distribution)	Corr: 0.925*** Aqmola: 0.929*** Nur sultan: 0.720***	Corr: 0.946*** Aqmola: 0.962*** Nur sultan: −0.518***	Corr: 0.473*** Aqmola: 0.482*** Nur sultan: 0.066	Srad
						(distribution)	Corr: 0.844*** Aqmola: 0.864*** Nur sultan: −0.343***	Corr: 0.673*** Aqmola: 0.700*** Nur sultan: 0.390***	ST
							(distribution)	Corr: 0.329*** Aqmola: 0.357*** Nur sultan: 0.614***	vs
								(distribution)	PET

Figure 6. Simple correlation between PET and environmental factors in Akmola State and the metropolitan area. *: $p < 0.1$; *** $p < 0.01$.
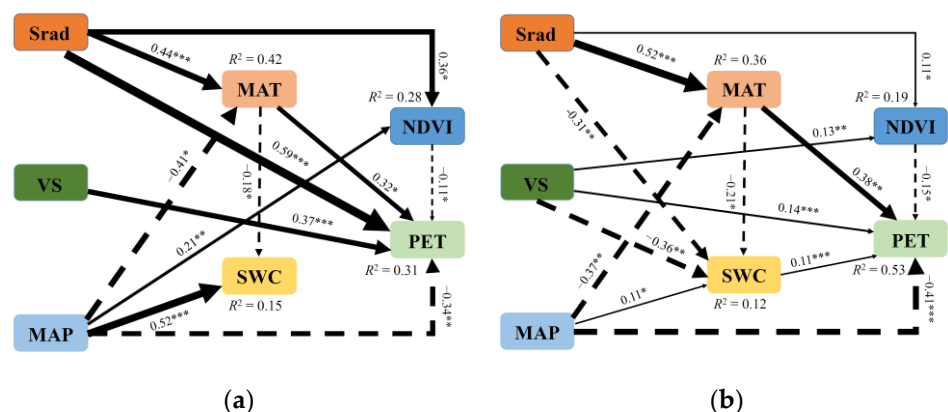
Figure 7. Spatial distribution of bias correlation coefficients between PET and environmental factors passing significance test throughout Akmola State: (**a**) PET and MAT bias correlation coefficient; (**b**) PET and NDVI bias correlation coefficient; (**c**) PET and SWC bias correlation coefficient; (**d**) PET and Srad bias correlation coefficient; (**e**) PET and ST bias correlation coefficient; and (**f**) PET and wind speed bias correlation coefficient.

Figure 7 depicts the relationships between PET and the various elements that passed the significance test, whereas the gray areas represent areas that failed the significance test (i.e., areas where they were not significantly correlated). MAT and PET demonstrated a significant positive correlation in the western part of the study area and, to a lesser extent,

in the eastern part (42.81% of the study area passed the significance test), with skewed correlation coefficients concentrated in the range of [0.32, 0.69], as shown in Figure 7a, with the strongest correlation between PET and MAT in the southwestern part of Akmola State and weaker correlations in the western, northern, and other parts of the state. The regional heterogeneity of the association between PET and NDVI in the studied area is evident. As depicted in Figure 7b, the area of PET and NDVI passing the significance test accounted for 6.29% of the state of Akmola, while the area of significant negative correlation accounted for 3.60% of the state, primarily in the state's northwest and middle east. The region with significant positive correlation accounted for 2.69% of the state of Akmola, primarily distributed in the south, middle, and east. Figure 7c illustrates the regional distribution of the PET–SWC partial correlation coefficients. The area that passed the significance test amounted to 56.44%, and the partial correlation coefficients fell between −0.76 and −0.32. The highest negative link between PET and SWC occurred in the southwestern portion of Akmola State, whereas the correlation was weaker in the middle and northern regions. As shown in Figure 7d, PET and Srad were predominantly positively correlated, with 94.58% of the area passing the significance test and biased relationships having values in the range of [0.32, 0.84], with the strongest positive correlation between PET and Srad in the southwest, followed by the central region, and the weakest correlation in the north. As depicted in Figure 7e, PET and ST were predominantly positively correlated, with 81.57% of the study area passing the significance test, having partial correlation coefficients in the range of [0.31, 0.78], with the strongest correlation between PET and ST in the central portion of the study area and the weakest correlation in the west. As shown in Figure 7f, PET and VS were predominantly positively correlated, with 64.02% of the area passing the significance test, with correlation coefficients in the range of [0.32, 0.85]. The strongest correlation between PET and VS was in the southwestern portion of the study area, and a significant decreasing spatial gradient of correlation coefficients can be observed from the southwestern to the northeastern direction.

3.2.4. Drivers of Potential Evapotranspiration Change in Akmola State

To further investigate the driving effects of different influencing factors on PET change in the study area, different climatic factors were screened through a covariance assessment. In this way, the importance of the contribution of different environmental factors to PET change was ranked, and the drivers of PET change in the study area were quantified by structural equation modeling (SEM). Figure 8 depicts the principal drivers of PET change in Akmola State and the metropolitan area.

Figure 8. SEM used to assess the effect of environmental factors on PET. The solid line represents a significant positive effect, the dashed line represents a significant negative effect and, if there is no significant relationship between variables, the line is omitted. *: $p < 0.1$; ** $p < 0.05$; *** $p < 0.01$.

Figure 8a demonstrates that the SEM analysis explained 31% of the PET variation in Akmola State. Srad (0.59 ***), VS (0.37 ***), and MAT (0.32 *) had a direct beneficial influence

on PET in Akmola, whereas NDVI (−0.11 *) and MAP (−0.34 **) had direct negative effects. In addition, we observed that NDVI and MAT had direct effects on PET changes, while Srad, VS, and MAP had direct and indirect effects on PET changes. As shown in Figure 8a, both Srad and MAP had direct effects on PET that were statistically significant, but also had favorable impacts on MAT and NDVI, leading to indirect effects on PET: Srad presented loadings of 0.44 *** and 0.36 * and MAP presented loadings of −0.41 * and 0.21 ** on MAT and NDVI, respectively.

Nursultan City and its surrounding areas (i.e., the capital circle) in Akmola Prefecture have been planted with huge areas of plantations since the 1990s, drastically altering the regional vegetation coverage. We employed SEM to investigate the driving mechanisms of local PET change. As depicted in Figure 8b, the interpretation of PET changes in the capital region by the model reached 53%, differing from overall Akmola State, in terms of the driving forces of PET changes. VT, SWC, and MAT had direct beneficial effects on PET in this location, with loadings of 0.14 ***, 0.11 ***, and 0.38 **, respectively; meanwhile, NDVI and MAP had direct detrimental impacts on PET, with loadings of −0.15 * and −0.41 **, respectively. In addition, NDVI, SWC, and MAT have direct impacts on PET, while VS and MAP presented both direct or indirect effects, and Srad had only indirect effects. As shown in Figure 8b, Srad has no direct significant impact on PET in the capital circle region, though it had an indirect impact on PET by affecting MAT, SWC, and NDVI (loadings of 0.52 ***, −0.31 **, and 0.11 *, respectively); VS not only directly promoted the increase in PET, but also exerted different effects on PET by inhibiting SWC and promoting the growth of NDVI. In a similar manner, MAP not only had direct negative impacts on PET, but also indirectly affected PET by reducing MAT and increasing SWC.

4. Discussion

The theoretical upper limit of real evapotranspiration (or PET) is an essential component of the energy balance. It is frequently employed in the analysis of dry and wet climate conditions, water resource management, agricultural water demand and production management, ecological and environmental governance, and the regional water cycle and water resources [27]. We calculated PET in the study area from 1991 to 2021 using the Penman-Monteith (P–M) model and analyzed its spatiotemporal changing characteristics. The results indicated that PET in the state of Akmola maintained a high value over time. The southwest of the state presented the highest values of PET, exceeding 1000 mm. Moreover, it is the only region in which PET grew from 1991 to 2021, whereas other regions showed a declining trend. Yan et al. (2022) have also noted that the Pan Central Asia Dry Area has become typically wetter since the middle of the 20th century, which contradicts Hypothesis 1 in this study [28]. It is influenced by the water vapor in the Atlantic Ocean and Arctic Ocean as a result of the northwest circulation [29]. The relative humidity of the air has increased throughout the entirety of Central Asia, lessening the likelihood of potential evapotranspiration. This demonstrates that the potential evapotranspiration is affected by regional and topographic variables, and that there are regional disparities in the impact of climate on PET in various locations [30].

Consistent with Hypothesis 2, partial correlation analysis and SEM analysis demonstrated that the primary drivers of PET change in Akmola were Srad and VS; in addition to SRAD, VS had a strong positive effect on PET ($p < 0.001$). An increase in wind speed will enhance air fluidity and hasten the evaporation of water. The typical annual precipitation in the study area is less than 500 mm, and increased rain substantially encourages the growth of PET [31]; In recent years, as the monsoon regional circulation system in Asia and India has weakened, the wind speed in Central Asia has decreased gradually [32,33] and the increase in aerosol concentration in the atmosphere has caused global dimming, which is the primary factor affecting the decrease in Srad. Significant causes of the decline in potential evapotranspiration in Akmola State are the aforementioned global influences, particularly the reduction in wind speed and solar radiation.

Changes in land cover, particularly in vegetation cover, have an effect on the regional microclimate [34]. In Akmola State, around the capital of Kazakhstan (Nur Sultan) and its adjacent areas, 879.7 km^2 of artificial forest have been planted since 1997, following more than 20 years of labor. This has had a significant impact on the environment of the capital circle. Using SEM, we estimated the driving effect of environmental elements in the capital circle region, in order to investigate the influence of anthropogenic land cover changes on local PET. Figure 8b demonstrates that VS was the primary driver of PET change near the capital circle, whereas Srad had no direct effect on PET in this location. Although PET in the capital circle was not directly or considerably affected by Srad, it was more strongly affected by other factors than in the rest of Akmola. Compared to the entire state of Akmola, SWC, MAT, and NDVI exerted a greater influence on PET near the capital. According to Wang et al. (2014), evapotranspiration in arid regions is extremely sensitive to soil surface water concentration [35]. When the soil surface is generally dry, there is a considerable positive correlation between evapotranspiration and soil water content. Significantly negative correlations exist between evapotranspiration and soil surface water content when the soil is relatively moist. In the hydrological balancing model proposed by Chen et al. (2008), groundwater recharge in the Huaihe River Plain accounted for 25% of the potential evapotranspiration [36]. The link between soil water content and PET varies with geography and climate. In the vicinity of the capital circle, Srad was seen to decrease the soil water content and have an indirect effect on PET. MAT had a greater influence on PET. Sudan has an abundance of groundwater resources, and the use efficiency of groundwater in this region has been improved by growing extensive tracts of artificial forests. Simultaneously, the MAP in the research area is also gradually growing. Under the condition of adequate water, a rise in temperature may extend the growing season of plants [37]. Through transpiration, when the NDVI increases, the local climate becomes wetter than the surrounding areas. This plays a significant part in the decrease in PET.

5. Conclusions

We used the P–M model to calculate and analyze the spatiotemporal distribution characteristics of PET in Akmola, a key agricultural and animal husbandry production center in Kazakhstan, and combined it with biased correlation analysis and SEM to investigate the driving factors of PET change in the study area. Simultaneously, we investigated the impact of meteorological activity on PET following the execution of the Green Environment Project in Kazakhstan's capital region. From 1991 to 2021, the data indicated that the multi-year average PET in Akmola was 835.87 mm, indicating a declining trend. Regarding the spatial distribution, PET exhibited a high degree of regional heterogeneity, being substantially greater in the southwest and northeast of the research area than in the center. The majority of meteorological activity in the study area had a substantial association with PET, and there was a high degree of spatial variation in the number of environmental factor–PET biased relationships. Similar regional characteristics characterized the links between PET and Srad, VS, and MAT, and the correlations were highest in the southwestern region of Akmola State. The spatial distribution of the associations between PET and SWC, and PET and ST were comparable, with the correlation being strongest in the center of the research area. The SEM indicated that Srad (0.59) and VS (0.37) were the primary determinants of PET change over the whole study region. With the expansion of man-made public forest space in the capital circle, the local environment has been enhanced; here, MAP is also a primary element influencing local PET change.

The present study calculates the spatial and temporal variation of potential evapotranspiration in Alamok Oblast, Kazakhstan for the last three decades at the regional scale, which is no longer limited to the estimation of PET at a single point scale and fills in the research on the variation of regional PET and the effect of its influence. The limitation is the lack of in-depth study of spatial and temporal distribution of meteorological data, and also the effect of local land cover type changes on PET should be studied in depth first Figure S1.

Supplementary Materials: The following supporting information can be downloaded at: https://www.mdpi.com/article/10.3390/rs14215311/s1, Figure S1: Comparison of satellite grid data and ground station data.

Author Contributions: Y.C. and S.Z. were the main contributors to this work. Y.C. and S.Z. are the co-first authors of this article. Y.C.: data curation; conceptualization; supervision; formal analysis. S.Z.: validation; software. Y.W.: funding acquisition; investigation. All authors commented on previous versions of the manuscript. All authors have read and agreed to the published version of the manuscript.

Data Availability Statement: The Meteorological data were obtained from the Terra Climate dataset published by the University of Iowa (https://doi:10.1038/sdata.2017.191, URL (accessed on 25 August 2022), which include global land surface, monthly mean climate, and climate water balance datasets, in addition to climate data such as Srad, PET, VS, MAP, VPD, and actual evapotranspiration. Land cover data were obtained from ESA's global land cover database with coverage at 300-m spatial resolution from 1992 to 2020 (https://cds.climate.copernicus.eu/cdsapp#!/dataset/satellite-land-cover, URL (accessed on 25 August 2022), which classifies the global land surface into 22 categories based on the UN FAO Land Cover Classification System (LCCS). NDVI data comes from USGS official website (https://glovis.usgs.gov/, URL (accessed on 25 August 2022). Other relevant data are listed in Table 1.

Conflicts of Interest: The authors declare no conflict of interest.

References

1. Koutroulis, A.G. Dryland Changes under Different Levels of Global Warming. *Sci. Total Environ.* **2019**, *655*, 482–511. [CrossRef] [PubMed]
2. Wang, X.; Zhang, J.; Shahid, S.; Guan, E.; Wu, Y.; Gao, J.; He, R. Adaptation to Climate Change Impacts on Water Demand. *Mitig. Adapt. Strateg. Glob. Chang.* **2016**, *21*, 81–99. [CrossRef]
3. Dai, Z.; Yu, M.; Chen, H.; Zhao, H.; Huang, Y.; Su, W.; Xia, F.; Chang, S.X.; Brookes, P.C.; Dahlgren, R.A. Elevated Temperature Shifts Soil N Cycling from Microbial Immobilization to Enhanced Mineralization, Nitrification and Denitrification across Global Terrestrial Ecosystems. *Glob. Chang. Biol.* **2020**, *26*, 5267–5276. [CrossRef] [PubMed]
4. Dai, A. Increasing Drought under Global Warming in Observations and Models. *Nat. Clim. Chang.* **2013**, *3*, 52–58. [CrossRef]
5. Berg, A.; Sheffield, J.; Milly, P.C.D. Divergent Surface and Total Soil Moisture Projections under Global Warming. *Geophys. Res. Lett.* **2017**, *44*, 236–244. [CrossRef]
6. Durán, J.; Delgado-Baquerizo, M.; Dougill, A.J.; Guuroh, R.T.; Linstdter, A.; Thomas, A.D.; Maestre, F.T. Temperature and Aridity Regulate Spatial Variability of Soil Multifunctionality in Drylands across the Globe. *Ecology* **2018**, *99*, 1184–1193. [CrossRef]
7. Maestre, F.T.; Benito, B.M.; Berdugo, M.; Concostrina-Zubiri, L.; Delgado-Baquerizo, M.; Eldridge, D.J.; Guirado, E.; Gross, N.; Kéfi, S.; Le Bagousse-Pinguet, Y. Biogeography of Global Drylands. *New Phytol.* **2021**, *231*, 540–558. [CrossRef]
8. Hu, Z.; Zhang, C.; Hu, Q.; Tian, H. Temperature Changes in Central Asia from 1979 to 2011 Based on Multiple Datasets. *J. Clim.* **2014**, *27*, 1143–1167. [CrossRef]
9. Gessner, U.; Naeimi, V.; Klein, I.; Kuenzer, C.; Klein, D.; Dech, S. The Relationship between Precipitation Anomalies and Satellite-Derived Vegetation Activity in Central Asia. *Glob. Planet. Chang.* **2013**, *110*, 74–87. [CrossRef]
10. Fisher, J.B.; Melton, F.; Middleton, E.; Hain, C.; Anderson, M.; Allen, R.; McCabe, M.F.; Hook, S.; Baldocchi, D.; Townsend, P.A. The Future of Evapotranspiration: Global Requirements for Ecosystem Functioning, Carbon and Climate Feedbacks, Agricultural Management, and Water Resources. *Water Resour. Res.* **2017**, *53*, 2618–2626. [CrossRef]
11. Oki, T.; Kanae, S. Global Hydrological Cycles and World Water Resources. *Science* **2006**, *313*, 1068–1072. [CrossRef] [PubMed]
12. Jung, M.; Reichstein, M.; Ciais, P.; Seneviratne, S.I.; Sheffield, J.; Goulden, M.L.; Bonan, G.; Cescatti, A.; Chen, J.; De Jeu, R. Recent Decline in the Global Land Evapotranspiration Trend Due to Limited Moisture Supply. *Nature* **2010**, *467*, 951–954. [CrossRef] [PubMed]
13. Jasechko, S.; Sharp, Z.D.; Gibson, J.J.; Birks, S.J.; Yi, Y.; Fawcett, P.J. Terrestrial Water Fluxes Dominated by Transpiration. *Nature* **2013**, *496*, 347–350. [CrossRef] [PubMed]
14. Yang, W.; Wang, Y.; Liu, X.; Zhao, H.; Wang, G.; Shao, R. Estimating the Evaporation in the Fenghuo Mountains Permafrost Region of the Tibetan Plateau. *Catena* **2020**, *194*, 104754. [CrossRef]

15. Ma, N.; Szilagyi, J.; Zhang, Y. Calibration-free Complementary Relationship Estimates Terrestrial Evapotranspiration Globally. *Water Resour. Res.* **2021**, *57*, e2021WR029691. [CrossRef]

16. Makori, D.M.; Abdel-Rahman, E.M.; Ndungu, N.; Odindi, J.; Mutanga, O.; Landmann, T.; Tonnang, H.E.Z.; Kiatoko, N. The Use of Multisource Spatial Data for Determining the Proliferation of Stingless Bees in Kenya. *GIScience Remote Sens.* **2022**, *59*, 648–669. [CrossRef]

17. El-Mageed, A.; Taia, A.; El-Mageed, A.; Shimaa, A.; El-Saadony, M.T.; Abdelaziz, S.; Abdou, N.M. Plant Growth-Promoting Rhizobacteria Improve Growth, Morph-Physiological Responses, Water Productivity, and Yield of Rice Plants under Full and Deficit Drip Irrigation. *Rice* **2022**, *15*, 16. [CrossRef]

18. Li, D. Assessing the Impact of Interannual Variability of Precipitation and Potential Evaporation on Evapotranspiration. *Adv. Water Resour.* **2014**, *70*, 1–11. [CrossRef]

19. Pascolini-Campbell, M.; Reager, J.T.; Chandanpurkar, H.A.; Rodell, M. Retraction Note: A 10 per Cent Increase in Global Land Evapotranspiration from 2003 to 2019. *Nature* **2022**, *604*, 202. [CrossRef]

20. Tegos, A.; Malamos, N.; Koutsoyiannis, D. RASPOTION—A New Global PET Dataset by Means of Remote Monthly Temperature Data and Parametric Modelling. *Hydrology* **2022**, *9*, 32. [CrossRef]

21. Ghiat, I.; Mackey, H.R.; Al-Ansari, T. A Review of Evapotranspiration Measurement Models, Techniques and Methods for Open and Closed Agricultural Field Applications. *Water* **2021**, *13*, 2523. [CrossRef]

22. Chen, C.; Zhang, X.; Lu, H.; Jin, L.; Du, Y.; Chen, F. Increasing Summer Precipitation in Arid Central Asia Linked to the Weakening of the East Asian Summer Monsoon in the Recent Decades. *Int. J. Climatol.* **2021**, *41*, 1024–1038. [CrossRef]

23. Hao, H.; Chen, Y.; Xu, J.; Li, Z.; Li, Y.; Kayumba, P.M. Water Deficit May Cause Vegetation Browning in Central Asia. *Remote Sens.* **2022**, *14*, 2574. [CrossRef]

24. Tadono, T.; Nagai, H.; Ishida, H.; Oda, F.; Iwamoto, H. Generation of the 30 m-mesh global digital surface model by alos prism. *Int. Arch. Photogramm. Remote Sens. S* **2016**, *XLI B4*, 157–162. [CrossRef]

25. Mensah, S.; du Toit, B.; Seifert, T. Diversity–Biomass Relationship across Forest Layers: Implications for Niche Complementarity and Selection Effects. *Oecologia* **2018**, *187*, 783–795. [CrossRef] [PubMed]

26. van der Sande, M.T.; Peña-Claros, M.; Ascarrunz, N.; Arets, E.J.M.M.; Licona, J.C.; Toledo, M.; Poorter, L. Abiotic and Biotic Drivers of Biomass Change in a Neotropical Forest. *J. Ecol.* **2017**, *105*, 1223–1234. [CrossRef]

27. Guo, L.; Cheng, J.; Luedeling, E.; Koerner, S.E.; He, J.-S.; Xu, J.; Gang, C.; Li, W.; Luo, R.; Peng, C. Critical Climate Periods for Grassland Productivity on China's Loess Plateau. *Agric. For. Meteorol.* **2017**, *233*, 101–109. [CrossRef]

28. Yan, X.; Zhang, Q.; Ren, X.; Wang, X.; Yan, X.; Li, X.; Wang, L.; Bao, L. Climatic Change Characteristics towards the "Warming–Wetting" Trend in the Pan-Central-Asia Arid Region. *Atmosphere* **2022**, *13*, 467. [CrossRef]

29. Chen, X.; Li, B.; Li, Q. Spatio-Temporal Pattern and Changes of Evapotranspiration in Arid Central Asia and Xinjiang of China. *J. Arid Land* **2012**, *4*, 105–112. [CrossRef]

30. Xu, C.-Y.; Singh, V.P. Evaluation of Three Complementary Relationship Evapotranspiration Models by Water Balance Approach to Estimate Actual Regional Evapotranspiration in Different Climatic Regions. *J. Hydrol.* **2005**, *308*, 105–121. [CrossRef]

31. Sun, J.; Wang, G.; Sun, X.; Hu, Z.; Lin, S.; Wang, F.; Yang, Y. New Cognition on the Response of Reference Evapotranspiration to Climate Change in China Using an Independent Climatic Driver System. *Agric. Water Manag.* **2022**, *262*, 107445. [CrossRef]

32. Zhang, Y.; Liu, C.; Tang, Y.; Yang, Y. Trends in Pan Evaporation and Reference and Actual Evapotranspiration across the Tibetan Plateau. *J. Geophys. Res. Atmos.* **2007**, *112*. [CrossRef]

33. Gong, D.-Y.; Ho, C.-H. The Siberian High and Climate Change over Middle to High Latitude Asia. *Theor. Appl. Climatol.* **2002**, *72*, 1–9. [CrossRef]

34. Singh, D.; McDermid, S.P.; Cook, B.I.; Puma, M.J.; Nazarenko, L.; Kelley, M. Distinct Influences of Land Cover and Land Management on Seasonal Climate. *J. Geophys. Res. Atmos.* **2018**, *123*, 12–17. [CrossRef]

35. Wang, C.; Wang, X.; Liu, D.; Wu, H.; Lü, X.; Fang, Y.; Cheng, W.; Luo, W.; Jiang, P.; Shi, J. Aridity Threshold in Controlling Ecosystem Nitrogen Cycling in Arid and Semi-Arid Grasslands. *Nat. Commun.* **2014**, *5*, 4799. [CrossRef] [PubMed]

36. Chen, X.; Zhang, Z.-C.; Zhang, X.-N.; Chen, Y.-Q.; Qian, M.-K.; Peng, S.-F. Estimation of Groundwater Recharge from Precipitation and Evapotranspiration by Lysimeter Measurement and Soil Moisture Model. *J. Hydrol. Eng.* **2008**, *13*, 333–340. [CrossRef]

37. Fang, C.; Ye, J.; Gong, Y.; Pei, J.; Yuan, Z.; Xie, C.; Zhu, Y.; Yu, Y. Seasonal Responses of Soil Respiration to Warming and Nitrogen Addition in a Semi-Arid Alfalfa-Pasture of the Loess Plateau, China. *Sci. Total Environ.* **2017**, *590*, 729–738. [CrossRef]